Influence of hydrothermal treatment on the surface characteristics and electrochemical behavior of Ti-6Al-4V bio-functionalized through plasma electrolytic oxidation

Fazel, M.; Salimijazi, H. R.; Shamanian, M.; Apachitei, I.; Zadpoor, A. A.

DOI
10.1016/j.surfcoat.2019.05.088

Publication date
2019

Document Version
Final published version

Published in
Surface and Coatings Technology

Surface & Coatings Technology 374 (2019) 222–231

Contents lists available at ScienceDirect

Surface & Coatings Technology

journal homepage: www.elsevier.com/locate/surfcoat

Influence of hydrothermal treatment on the surface characteristics and electrochemical behavior of Ti-6Al-4V bio-functionalized through plasma electrolytic oxidation

M. Fazel[a,b,*], H.R. Salimijazi[a], M. Shamanian[a], I. Apachitei[b], A.A. Zadpoor[b]

[a] Department of Materials Engineering, Isfahan University of Technology, Isfahan 84156-83111, Iran
[b] Department of Biomechanical Engineering, Delft University of Technology, Mekelweg 2, 2628 CD Delft, the Netherlands

ARTICLE INFO

Keywords:
Plasma electrolytic oxidation (PEO)
Hydrothermal treatment
Electrochemical impedance spectroscopy
Hydroxyapatite nanocrystals

ABSTRACT

The performance of biomaterials in general and orthopaedic biomaterials in particular is dependent on both the chemistry and topography of their surfaces. It is therefore important to tailor both of those aspects through an appropriate surface modification technique. Here, we examined the influence of hydrothermal treatment on the surface characteristics and electrochemical behavior of Ti-6Al-4V specimens whose surfaces were modified using plasma electrolytic oxidation (PEO). Even though no calcium-phosphorous related crystalline compound was identified in the XRD spectra of PEO layers, hydroxyapatite crystals were clearly detectable after the applied hydrothermal treatment. The partial water absorption of the HA crystals and their needle-like morphology resulted in a significant increase in the wettability of the surfaces. However, the application of post-PEO hydrothermal treatment also decreased the corrosion resistance of the PEO layers. The numerical results of electrochemical impedance spectroscopy demonstrated that the optimized surface properties and corrosion resistance were achieved in one of the groups, namely PEO-HT3, where the HA nanocrystals homogenously covered the entire surface of the specimens.

1. Introduction

Orthopaedic and dental implants are often manufactured from titanium-based alloys [1–3]. This is due to their unique physical and mechanical properties, such as high strength to weight ratio, superior corrosion resistance, and good biocompatibility [4–6]. However, the native oxidized, stressed, and contaminated surface resulting from the conventional manufacturing processes of titanium implants is not appropriate for biomedical applications [7,8]. Similar to other conventional metallic biomaterials, titanium alloys are classified as bio-inert, meaning that they are designed to not elicit any undesirable effects [9]. An appropriate surface modification method should be able to not only retain the great bulk properties of titanium alloys but also further enhance some specific surface-related properties that could be essential for biological applications [10,11]. In this respect, various types of surface treatment techniques have been investigated to improve the integration of implants in the bony environment. Different mechanical and chemical treatments such as blasting, acid etching, and simple anodic oxidation have, therefore, been applied to generate a rough implant surface while increasing the contact area and physical cell adhesion [11–14]. There are also various techniques for attaching bioactive compounds onto implants surfaces. These techniques include plasma/thermal spraying, electrophoretic deposition, and sol-gel [4,15–17]. In particular, it has been consistently shown that the presence of hydroxyapatite (HA) on the surface of titanium alloys has the potential of improving the osseointegration of orthopaedic implants [18–20]. Recently, researchers have proposed that the synergistic effects of surface chemistry and topography could be very effective for achieving a more stable bond between the surrounding bony tissue and the implant surface [21–24]. One of the approaches in this respect is the formation of an HA layer using plasma/thermal spraying techniques on previously roughened surfaces [4,15]. It has also been reported that large amounts of tricalcium phosphate (TCP) particles can be deposited on an anodized surface using the electrophoretic deposition technique [16]. However, the adhesion of these kinds of deposited coatings is often not satisfactory [19]. The coating could therefore be severely damaged through the mechanically demanding procedures that are often required for the implantation of (uncemented) implants.

A recently developed PEO technique allows for the fabrication of rough and porous coatings enriched with bioactive elements present in

* Corresponding author at: Department of Materials Engineering, Isfahan University of Technology, Isfahan 84156-83111, Iran.
E-mail address: mohammad.fazel@ma.iut.ac.ir (M. Fazel).

https://doi.org/10.1016/j.surfcoat.2019.05.088
Received 26 April 2019; Received in revised form 27 May 2019; Accepted 31 May 2019
Available online 03 June 2019
0257-8972/

the electrolyte [25,26]. The chemical composition of the electrolyte, therefore, significantly influences the behavior of the resulting PEO layers. This process consists of individual plasma discharge events that collectively give rise to the growth of a firmly attached oxide layer with a specific chemistry and microstructure [27–29]. It has, however, been reported that the incorporated Ca and P ions are usually dissolved within the titanium oxide matrix of the PEO layers [30–33]. A few other studies have shown a mixture of some crystalline phases such as TCP, HA, and $CaTiO_3$ that are formed through the PEO process [34,35]. Even when a specific electrolyte developed for osteointegrative coatings [34] has been used for PEO treatment, only a very minor amount of low-crystallized or amorphous apatite is formed in the coating [21].

The application of a post-PEO hydrothermal treatment (HT) enables the dissolved ions to interact with each other and to form a highly crystalline hydroxyapatite phase. Song et al. [36] have shown that post-PEO hydrothermal treatment is an effective way for forming HA crystallites on top of oxide layers. Chen et al. [33] have demonstrated that the improved cell response of hydrothermally treated samples is attributed to two factors. The first factor is the presence of Ca and P ions in the early stages of cell adhesion while the second factor is the HA pillars that could mechanically stimulate the cells to continue flattening and spreading on the surface. They have also reported that high surface stress caused by the formation of HA pillars can further stimulate the cell adhesion. It has been also reported that the nanopillars formed on the titanium surface are able to decrease biofilm formation [37]. It can, therefore, be concluded that post-PEO HT treatment not only is capable of maintaining the previously formed porous structure, but can also create a more favorable topography through the formation of HA crystals. This kind of stresses can, however, increase the surface energy, thereby influencing some other key properties such as the corrosion resistance. In this study, we created PEO layers using a calcium acetate-calcium glycerophosphate electrolyte and the constant current-constant voltage technique. Different surface properties such as the morphology, phase structure, wettability, and the electrochemical behavior of the PEO-treated samples before and after the applied HT treatment were also investigated to find the conditions giving rise to the best surface properties.

2. Experimental

Disk-type specimens (14 mm in diameter and 3 mm thick) were cut from a biomedical-grade (grade 23-ELI) Ti-6Al-4V rod. The surfaces of the as-received specimens were first ground using SiC abrasive papers (down to 1200#) and then polished using alumina powder (diameter = 0.5 μm) on a wet pad. Prior to the PEO treatment, the specimens were ultrasonically cleaned in ethanol and distilled water. The surface of the specimens was then oxidized using a PEO treatment where a stainless-steel plate was used as the cathode. The PEO process was performed in an electrolyte consisting of 0.02 M calcium acetate (Sigma–Aldrich, 114460-21-8) and 0.02 M calcium glycerophosphate (Sigma–Aldrich, 58409-70-4). A constant current-constant voltage method was employed to form the oxide layers, where the unipolar electric rectangular pulses were generated using a pulsed-DC power supply. In the first stage, a constant current of 20 A/dm^2 at a pulse frequency of 1 kHz and a positive duty cycle of 80% was applied. When the anodic potential reached the target voltage (470 V), the process was continued in the potentiostatic mode for 20 min. Finally, the PEO-treated specimens were rinsed in distilled water and dried in warm air. Two groups of the PEO-treated specimens were vertically placed in a high-pressure autoclave containing 300 ml alkaline water (pH = 11) and hydrothermally treated at 200 °C for 3 (group PEO-HT3) or 6 (group PEO-HT6) hours.

A scanning electron microscope (SEM; JSM-6500F, JEOL, Tokyo, Japan) equipped with energy-dispersive X-ray spectroscopy (EDS) was used to investigate the morphology and the chemistry of the oxidized samples.

X-ray diffraction profile was determined using a Philips X'pert MPD diffractometer, employing Cu K_α radiation (40 kV and 40 mA) at brag angles of 20–80°.

The wettability of the coatings was measured using high purity water droplets of 2 μl in volume. Images were collected using a video camera to measure the contact angle (ImageJ 1.51 k software).

Electrochemical experiments including the potentiodynamic polarization test and electrochemical impedance spectroscopy (EIS) were performed using a Potentiostat/Galvanostat device (model PARSTAT 2273) equipped with the PowerSuite software. A standard three-electrode cell was applied for the electrochemical tests where titanium specimens, a platinum electrode, and a saturated Ag/AgCl electrode were used as the working, auxiliary, and reference electrodes, respectively.

The specimens (with 1 cm^2 exposed surface area) were immersed in the Ringer's solution (8.6 g/l NaCl, 0.33 g/l $CaCl_2.2H_2O$ and 0.3 g/l KCl) at 37 ± 1 °C with a resting time of 60 min, which was required to allow for the open circuit potential (OCP) to be stabilized. The potentiodynamic polarization experiments were carried out where the scan rate was 1 mV s^{-1} in the range of −250 mV (vs. OCP) to +1000 mV. The impedance spectra were obtained in the frequency range from 100 kHz to 10 mHz at a bias potential of 10 mV. The EIS data was fitted to an equivalent electric circuit model using the Z-view software.

3. Results and discussion

3.1. Surface characterization and thickness measurements

SEM micrographs of PEO layers before and after hydrothermal treatment are shown in Fig. 1. A porous and rough oxide layer was created on the basis of swarming micro-discharges, which has been previously reported [29]. Despite the presence of numerous pores in the range of < 1 μm and > 3 μm, the majority of the pores were in the range of 1–3 μm, which is the most appropriate pore size to enable bonding with the globular bone matrix [21,28]. Ribeiro et al. [38] have reported that even though some cytoplasmic extensions penetrate such porosities, some others tend to create bridges across them. This could be attributed to the difference in the chemistry and the distribution of different phases between the top surface and the inside of the porosities.

The EDS analysis of the PEO layers (Fig. 2) showed the presence of oxygen within the anodic film, along with Ti, Al, and V that originate from the substrate as well as P and Ca that are incorporated from the PEO electrolyte. Even though different theories are proposed to explain the mechanisms through which ionic species from the electrolyte are incorporated into the coatings [39–42], the effects of the plasma state occurring in the solution during the PEO process seem to be the most dominant ones [43]. The presence of calcium ions within the anodic oxide layer, despite their positive charge, strongly supports this explanation. Furthermore, it is reasonable to assume that the electrophoretic force of the positively charged titanium specimen results in the adsorption of the phosphate anions from the electrolyte. Therefore, a combination of plasma discharges and the electrophoretic mobility of the anionic species during the PEO process caused a high concentration of calcium and phosphorous in the outermost surface of the PEO-treated specimens.

Since it is very difficult for the phosphate ions to diffuse from the inner parts of the oxide layer towards the surface, a higher amount of phosphorous is required in the coating to interact with the calcium ions and form hydroxyapatite during the hydrothermal treatment [36]. As is seen in Fig. 2, even though the atomic percentage of P did not change in different groups, the Ca content significantly increased after the hydrothermal treatment, where Ca/P ratio reached 1.67 for the group PEO-HT6. Fig. 3 shows that Ca and P were well distributed at the center of the PEO layer as well as on the top surface. However, after the hydrothermal treatment, a higher amount of these elements (especially calcium) was visible underneath the surface. This suggests that through

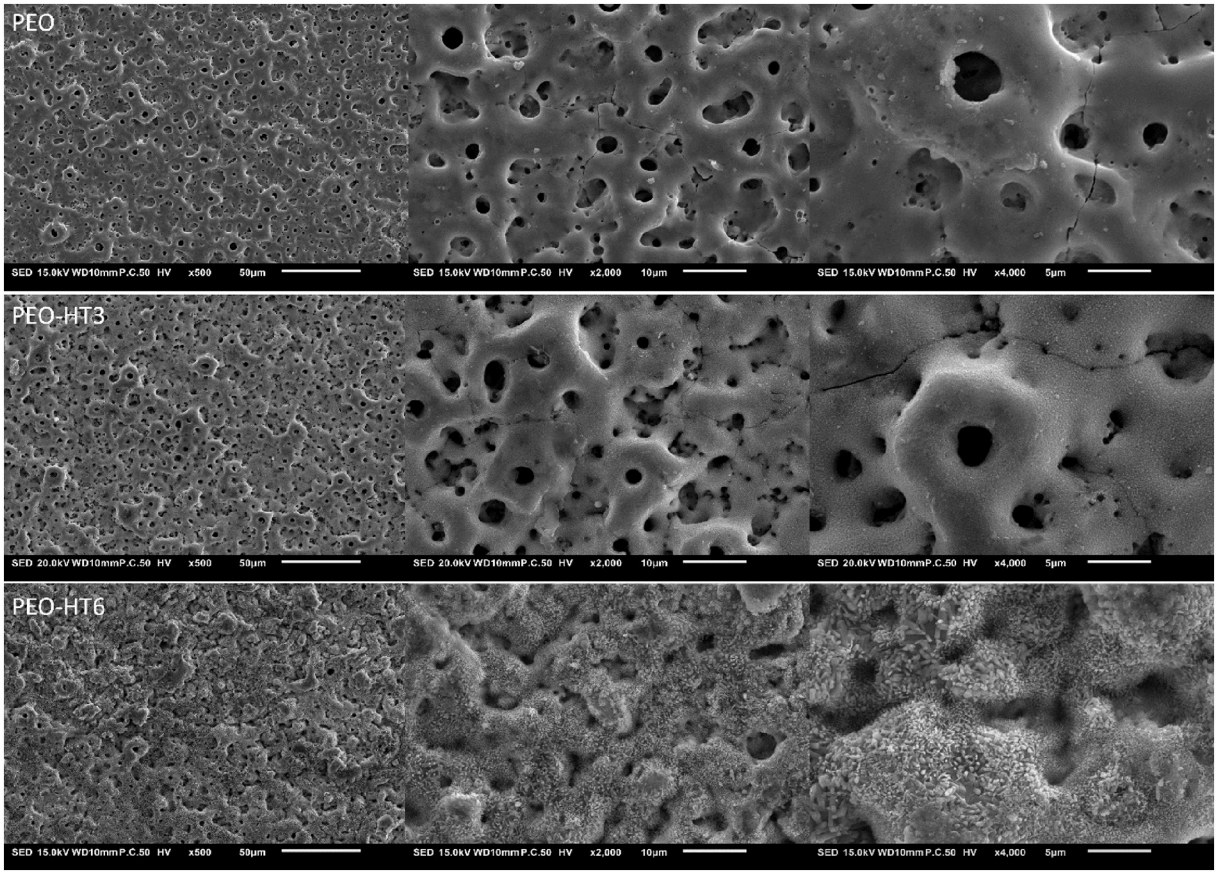

Fig. 1. The SEM micrographs of the PEO layers before and after 3 h (PEO-HT3) and 6 h (PEO-HT6) of hydrothermal treatment.

the HT treatment, the calcium ions move from the center of the oxide layer towards the surface, which is in line with what has been reported by others [36]. In other words, the aim of the hydrothermal treatment is to recrystallize previously incorporated calcium and phosphorous ions in the PEO layer. As a result of 3 h of this treatment, the surface was completely covered with a large number of HA nanocrystals (Fig. 1). The supersaturation of Ca^{2+}, PO_4^{3-}, and OH^- ions (from the hydrothermal environment) provides an appropriate condition for homogeneous nucleation all over the surface. Once the nucleation process is concluded, the growth process becomes dominant and HA nanocrystals preferably grow along the *c*-axis [44]. Therefore, a mixture of larger needles and pillars of hydroxyapatite (0.5–5 µm in length and 50–800 nm in diameter) appeared on the surface of the specimens from the PEO-HT6 group (Fig. 1). The formation of tightly bonded HA crystals inside the pores, as well as on the top surface provides a developed structure of PEO layers on the surface.

PEO-HT3, and PEO-HT6 groups.

Fig. 4 shows the evolution of the XRD pattern through the hydrothermal treatment of PEO layers. PEO layers mainly contained anatase (A) and rutile (R) TiO_2 accompanied by titanium peaks from the substrate (T). Even though Ca and P were detected in the EDS analysis, they appear to have been dissolved throughout the titanium oxide matrix without formation of any significant crystalline phase, which is in agreement with the results of other studies [23,45]. However, after hydrothermal treatment, the peaks related to hydroxyapatite crystals appeared in the spectra (Fig. 4). Because the hydrothermal solution was completely free of calcium and phosphorus, the crystalline structure of hydroxyapatite was formed through the interaction of previously incorporated calcium and phosphate ions under high-temperature and high-pressure steam water.

The wettability of the PEO and PEO-HT groups were investigated by measuring the static water contact angles (Fig. 5). Given the fact that inside the human body, the first contacts occur between the implant surface and the body fluids, the hydrophilicity of the surface is one of the most important factors influencing the cell response. As is seen in Fig. 5, the hydrothermal treatment significantly increased the wettability of the surface. It should be noted that the surface wettability is controlled by surface chemical structure and topography. It has been shown that the hydrophilicity and the cell adhesion increase as the roughness of HA increases [46]. Formation of HA crystals in sample PEO-HT6 provided a developed hybrid micro-nano topography with a relatively large contact area and surface energy that significantly modified the wettability of the surface. However, for the PEO-HT3 group, the water droplet spread out on the surface after 15 s. This suggests that, in addition to the effects of surface topography, the chemical structure of HA crystals and their hydrophilic nature also influences the surface wettability of the specimens [47,48]. The presence of hydrophilic Ca^{2+} and PO_4^{3-} components in the oxide layer resulted in a more surface hydration and therefore, the lower contact angles.

3.2. Corrosion behavior

Potentiodynamic polarization plots are presented in Fig. 6. As is clear from this figure, the PEO process caused a positive shift towards more noble potentials. It could, therefore, be concluded that the PEO process decreases the corrosion tendency of the Ti-6Al-4V alloy thermodynamically. Moreover, the anodic part of the polarization curves shifted towards lower corrosion current densities, indicating a higher corrosion resistance can be obtained, if anodic reactions are restricted in the PEO-treated specimens.

The PEO-HT3 group showed a slightly lower corrosion potential than of the PEO-treated specimens, while the E_{corr} values dropped to −20 mV after 6 h of hydrothermal treatment.

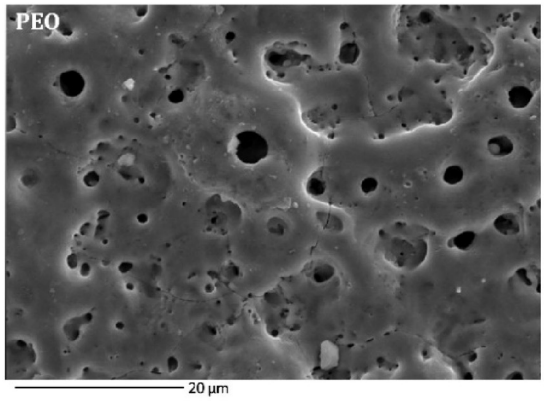

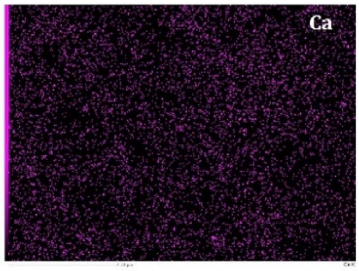

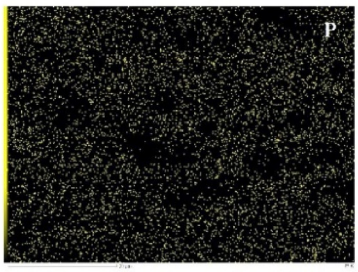

Element	O	Ti	Al	V	Ca	P
Wt. %	37.4	38.3	2.1	1.3	12.6	8.2
At. %	61.3	30	2.0	0.6	8.2	6.9

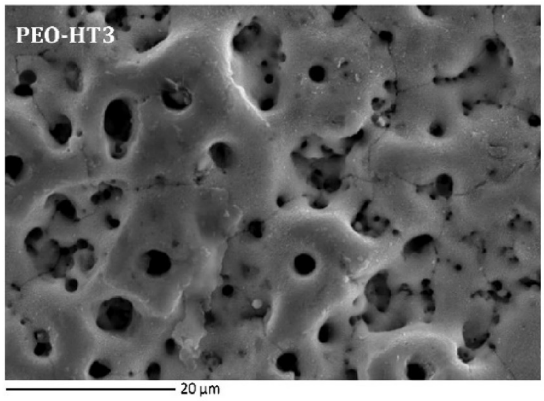

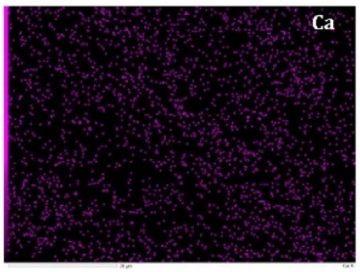

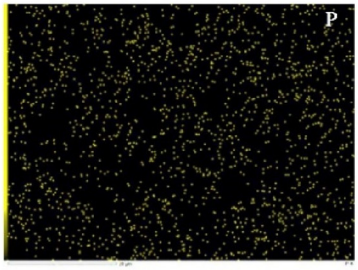

Element	O	Ti	Al	V	Ca	P
Wt. %	43.0	31.3	1.4	1.0	14.9	8.4
At. %	66.1	16.1	1.1	0.5	9.2	7.0

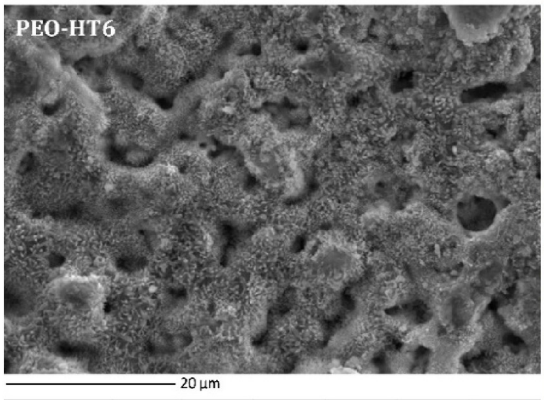

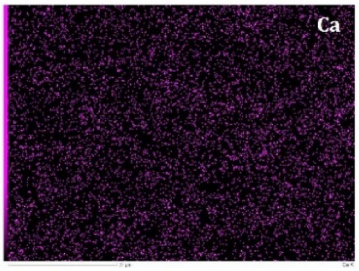

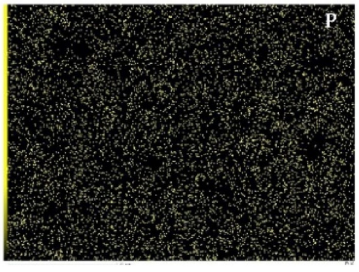

Element	O	Ti	Al	V	Ca	P
Wt. %	42.4	28.5	0.6	0.9	18.9	8.7
At. %	65.6	14.7	0.5	0.5	11.7	7.0

Fig. 2. The elemental composition obtained using EDS maps and the spectrum analysis of the top surface of the specimens from the PEO, PEO-HT3, and PEO-HT6 groups.

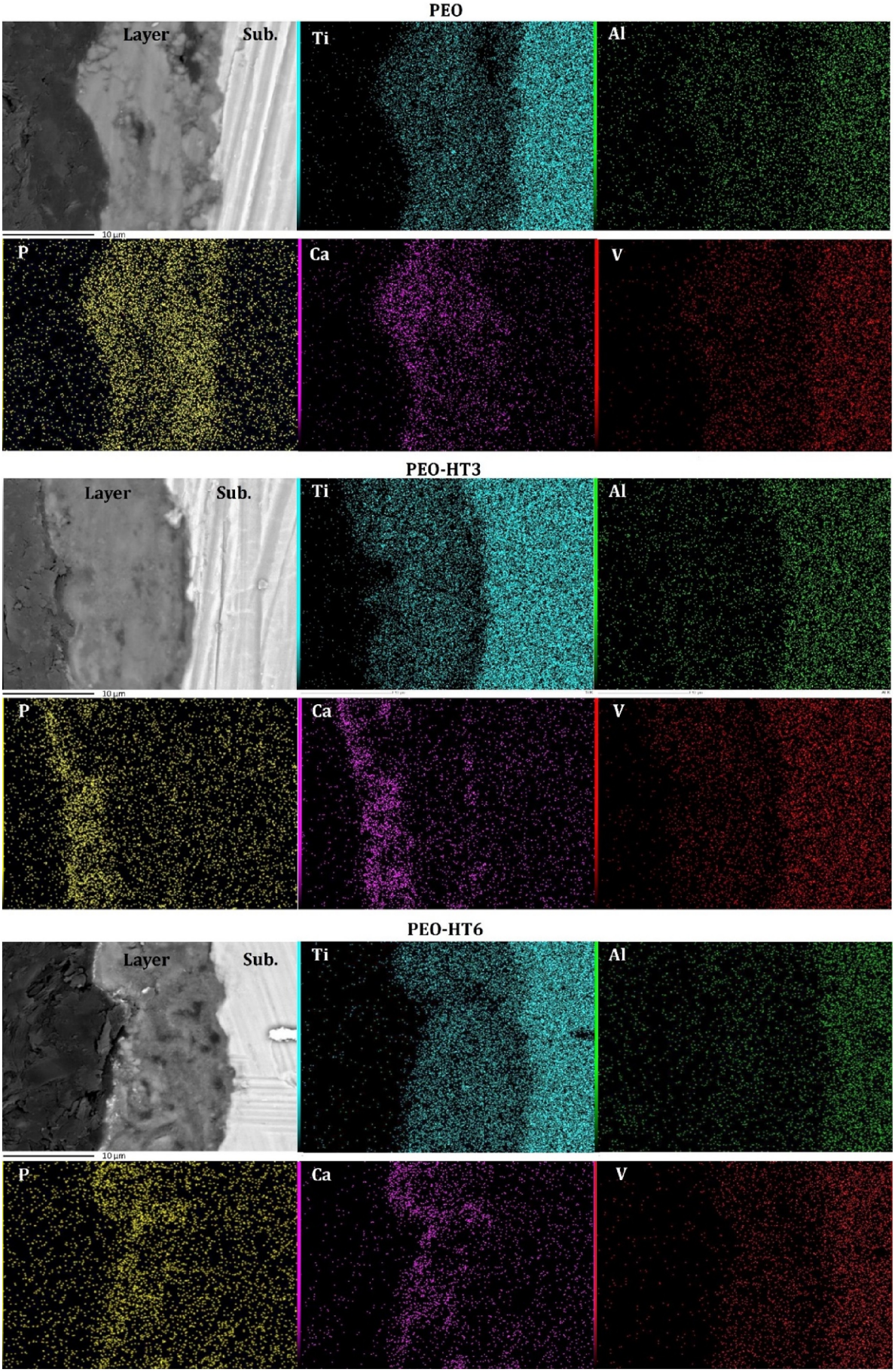

Fig. 3. Cross-sectional SEM micrographs and EDS elemental maps of the specimens from the PEO,

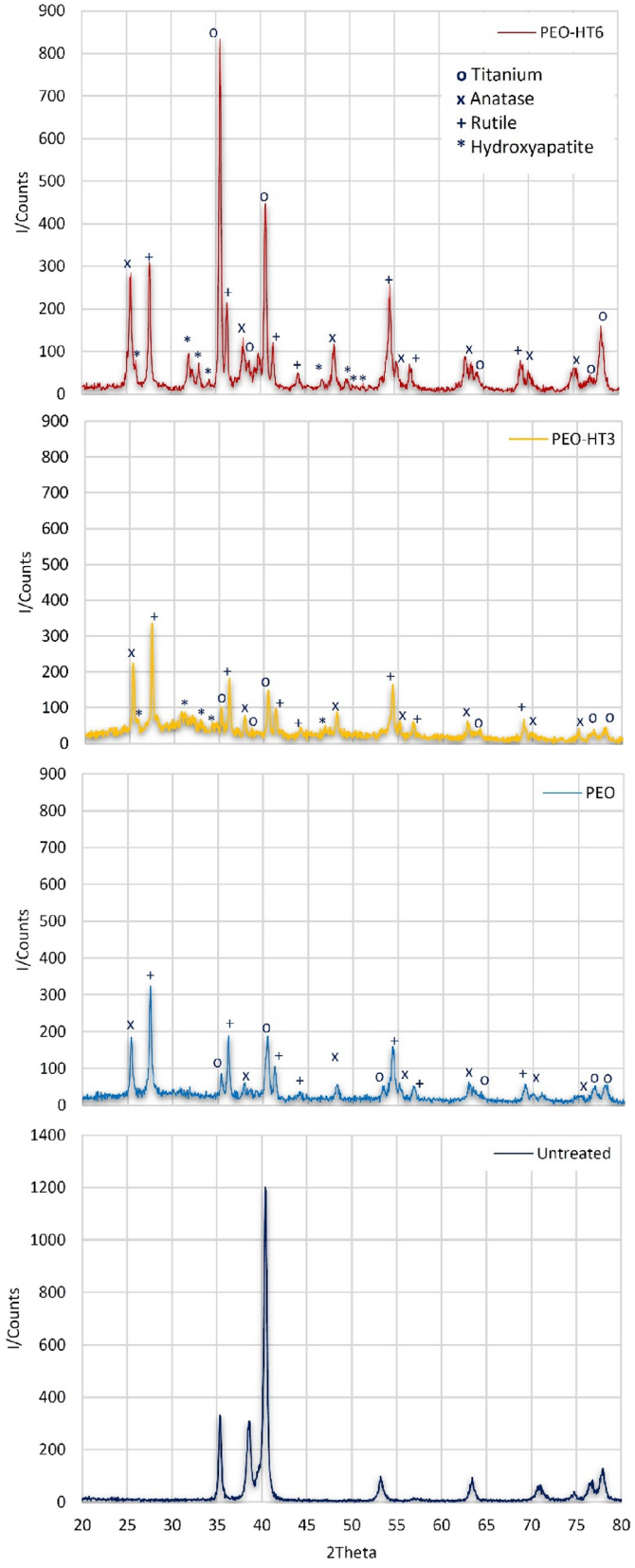

Fig. 4. The XRD patterns of the Ti-6Al-4V substrate and the PEO-treated specimens before and after the application of the hydrothermal treatment (T: Ti, A: anatase, R: rutile, H: hydroxyapatite).

A similar behavior was also observed for the corrosion and passive current densities (Table 1), where j_{corr} and j_p decreased from 0.05 μA·cm^{-2} and 0.71 μA·cm^{-2} for the group PEO-HT3 to 0.112 μA·cm^{-2} and 1.7 μA·cm^{-2} for the group PEO-HT6, respectively. Furthermore, the specimens from the PEO-HT6 group showed an unstable passive behavior, as the values of the corrosion current density continuously increased with the potential (Fig. 6). The different polarization behaviors of the hydrothermally-treated samples are mainly caused by their different surface topographies and structures. On the one hand, HA crystals were formed under the interaction of dissolved calcium and phosphate ions. The dissolved ions should have therefore moved from the inner parts of the oxide layer towards the surface, thereby leaving some vacancies and defects at their original location that has led to a reduction in the corrosion resistance. On the other hand, the stresses released by the growth of nano-sized HA spicules to thicker pillars may have also created different kinds of mechanical defects, which facilitated the diffusion of aggressive ions and accelerated the degradation of the oxide layer [49].

To investigate the influence of the applied hydrothermal treatment on the physical structure and corrosion properties of PEO layers, electrochemical impedance spectroscopy measurements were also conducted in the Ringer's solution (Fig. 7). There are at least two time constants in the Nyquist and Bode plots both before and after the hydrothermal treatment that represent the double-layer structure of the PEO coatings. The time constant appearing in the low-frequency range represents the properties of the inner barrier layer while the one present in the higher frequencies corresponds to the responses of the outer porous layer.

The values of the EIS parameters were obtained by fitting the electrical equivalent circuit (Fig. 8) to the experimental data. As no new layers were deposited in the case of the hydrothermally treated specimens and the HA needles formed through the already existing layers, the same circuit model with different parameter values was used. Furthermore, constant phase elements (Q) with non-ideal capacitive responses were used instead of pure capacitance to achieve better fitting results. The constant phase element (Q) acts as a capacitor when the impedance parameter (n) is equal to 1. For $n = 0$, Q is a real resistor and for $n = 0.5$, it acts as a Warburg element. The electrical elements of the proposed model include the solution resistance (R_s), the porous layer resistance (R_p), the barrier layer resistance (R_b), the constant phase elements for the porous (Q_p) and barrier (Q_b) layers, respectively, as well as a constant phase element (Q_d) that was added in-series to R_b to describe the diffusion of ions through the PEO layer.

The Nyquist plots showed a diagonal line with a slope of 45° for all the groups, indicating the indefinite length diffusion of the barrier layer. According to Table 2, the constant phase elements related to the barrier layer (Q_b) represents an indefinite length Warburg diffusion, where the impedance parameter (n_b) values are close to 0.5. Furthermore, the more compact structure of the inner layer can be concluded from the fitting results, where the real part of barrier layer resistance is much higher than the values related to the porous layer.

According to the numerical data (Table 2), the resistance of the porous layer in the PEO-HT3 group (61,500 Ω·cm^2) was almost 25 times higher than that of the group PEO-HT6 (2400 Ω·cm^2). This observation suggests that the nucleated nanocrystals through the oxide layer filled some of the porosities and cracks at the first stage. However, with the domination of the growth process and formation of the larger pillars, new physical and mechanical defects appeared through the oxide layer and caused a remarkable decrease in the cohesion of the outer layer.

However, the polarization resistance, which is inversely proportional to j_{corr} [35], can be defined as the sum of R_p and R_b. Since the barrier layer has much higher values of resistance as compared to the porous layer, the corrosion current density of the coatings strongly depends on the properties of the barrier layer. There are also big differences between the capacitance and resistance values of the barrier layers. If the Bode $|Z|$ plot is divided into two parts, the lower

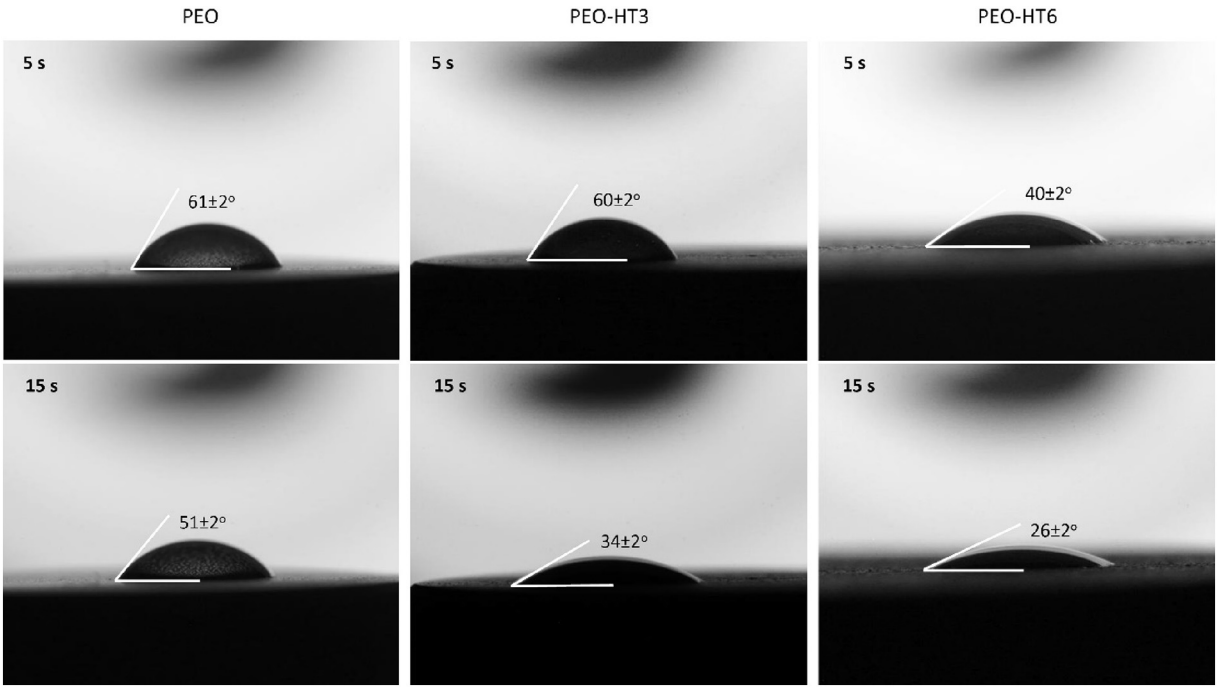

Fig. 5. The water contact angle of the specimens from the PEO, PEO-HT3, and PEO-HT6 groups after 5 and 15 s.

impedance values of the hydrothermally treated specimens at low frequencies (< 1–10 Hz), clearly show a significant decrease in the resistance of the barrier layer. Indeed, after 3 h of hydrothermal treatment, R_b decreased from 2.9 MΩ·cm^2 to 0.6 MΩ·cm^2 for the group PEO-HT3 and to 0.07 MΩ·cm^2 for the group PEO-HT6. This could be attributed to the ionic diffusion from the inner barrier layer that reduces the high density of this layer. In other words, by increasing the duration of the hydrothermal treatment, Ca^{2+} and PO_4^{3-} ions start to diffuse from the lower parts of the oxide layer. After 6 h of hydrothermal treatment, some imperfections are left behind within the inner barrier layer and reduce its protective behavior. Therefore, it can be concluded that the corrosion resistance of the specimens from the group PEO-HT6

Table 1
The polarization data measured for the specimens from the untreated, PEO, and PEO-HT groups.

Parameter	Group			
	Ti6Al4V	PEO	PEO-HT3	PEO-HT6
E_{corr} (mV)	−415	240	195	−25
j_{corr} (μA·cm^{-2})	0.140	0.023	0.050	0.112
j_p (μA·cm^{-2})	3.98	0.23	0.71	1.70

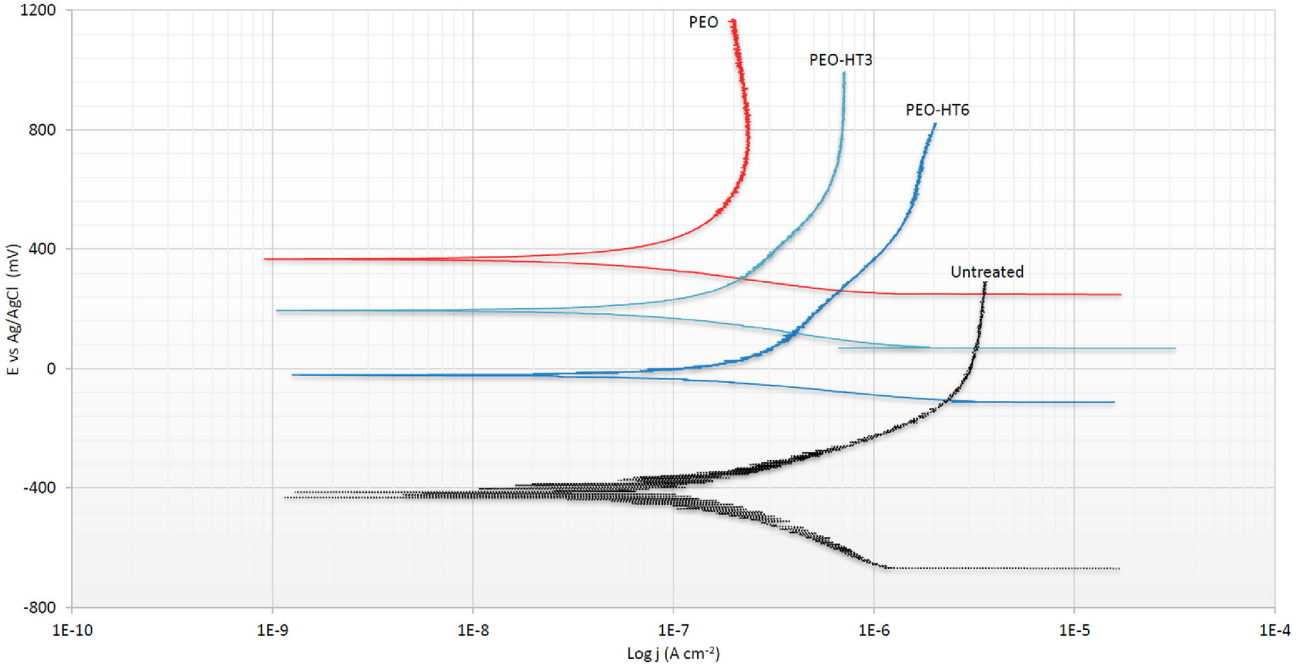

Fig. 6. The potentiodynamic polarization plots of the specimens from the untreated, PEO-treated, and PEO-HT-treated specimens.

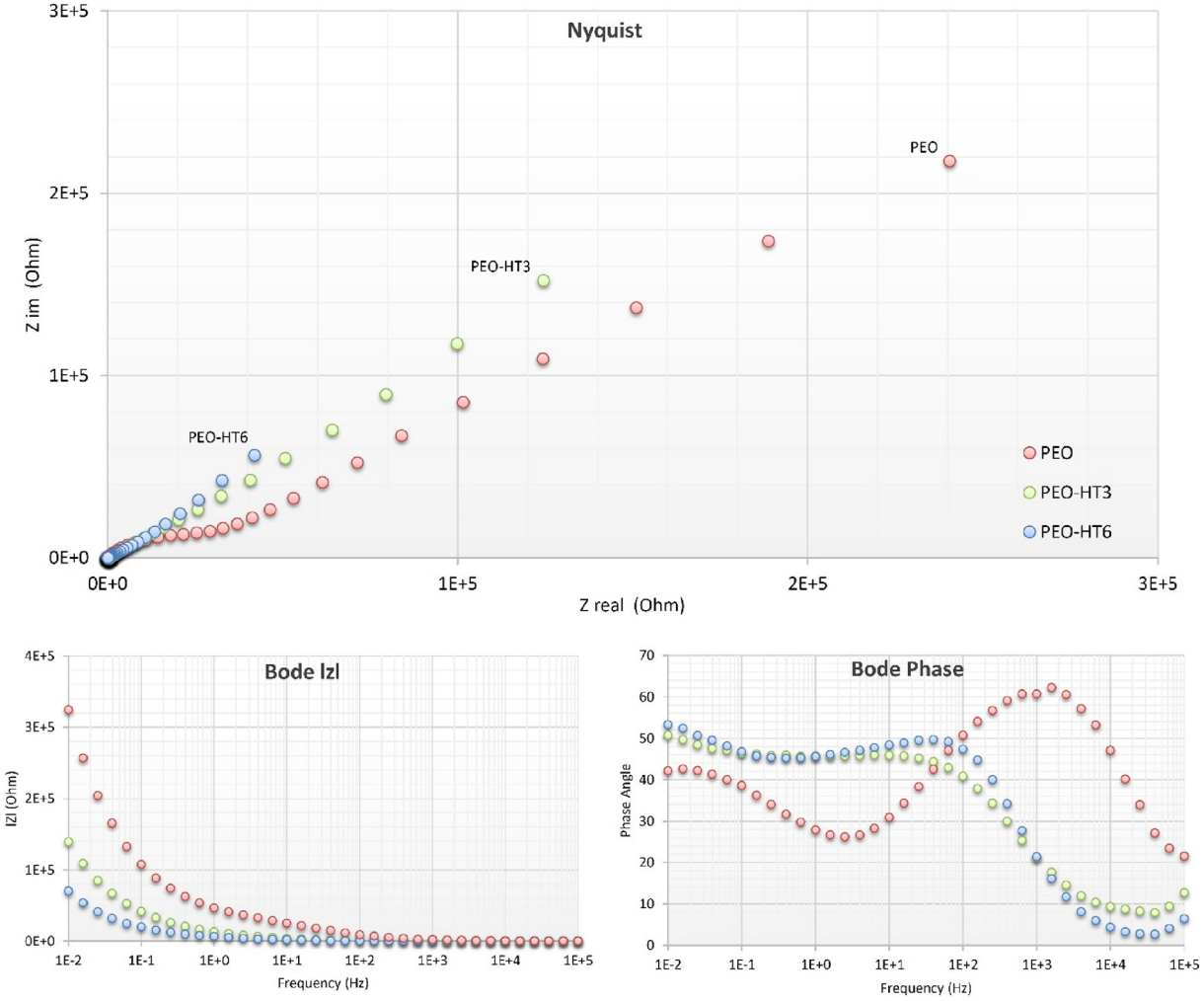

Fig. 7. The Nyquist, Bode phase angle, and Bode impedance plots corresponding to the EIS experiments of the specimens from the PEO and PEO-HT-treated groups.

was significantly lower than both other groups, which also agrees with the results of the potentiodynamic polarization curves. It should, therefore, be noted that even though the formation of HA crystals can improve the surface properties and cell adhesion [33,36], they could also make the surface more prone to energy-related phenomena such as corrosion. Consequently, it is important that the right balance between a protective layer and the formation of HA crystals is maintained through optimization of the parameters of both surface treatment

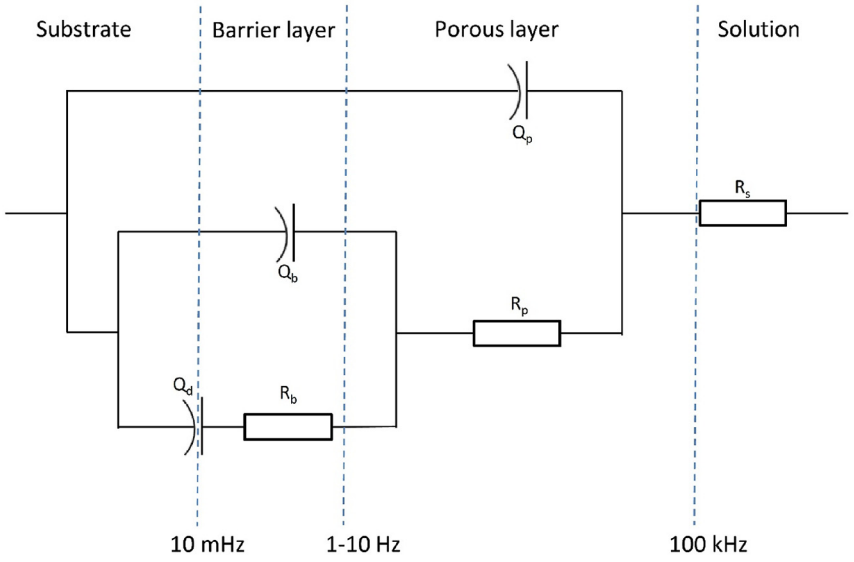

Fig. 8. The equivalent electrical circuit used for the fitting of the impedance data.

Table 2
The equivalent circuit parameters of the PEO layers before and after the applied hydrothermal treatment.

Group	Parameter									
	R_s (Ω·cm^2)	Q_p (S s^{-n} cm^{-2})	n_p	R_p (Ω·cm^2)	Q_b (S s^{-n} cm^{-2})	n_b	R_b (Ω·cm^2)	Q_d (S s^{-n} cm^{-2})	n_d	χ^2
PEO	162	6.84E–9	0.750	30,000	1.55E–9	0.552	2.9E6	5.04E–8	0.630	1.3E–4
PEO-HT3	190	8.35E-9	0.597	61,500	2.34E-8	0.569	6.1E5	5.95E-6	0.920	1.8E-4
PEO-HT6	152	6.10E–7	0.778	2400	9.98E–9	0.541	0.7E5	2.66E–6	0.825	1.5E–4

processes. In this respect, PEO-HT3 group showed a developed surface structure, which was completely covered with hydroxyapatite nanocrystals and also revealed a good corrosion resistance in the Ringer's solution.

4. Conclusions

Rough and porous PEO layers containing Ca and P elements were successfully synthesized on Ti-6Al-4V specimens, but no calcium-phosphorous related crystalline compounds were detected in the X-ray diffraction patterns. However, after hydrothermal treatment, homogenously distributed HA nanocrystals were formed through the porous PEO layer. XRD spectra of the specimens from the PEO-HT3 and PEO-HT6 groups demonstrated a mixed structure of HA, anatase, and rutile phases on the surfaces treated by both PEO and HT. The presence of the HA crystals caused a remarkable increase in the wettability of the hydrothermally treated groups. However, the corrosion resistance of the specimens from the PEO-HT6 group was significantly lower than that of both other groups, which is attributed to the formation of defects after growing HA nanocrystals to larger and thicker pillars. The specimens from the PEO-HT3 group showed both high corrosion resistance and uniform coverage of their surface by HA nanocrystals.

References

[1] S.A. Yavari, B.S. Necula, L.E. Fratila-Apachitei, J. Duszczyk, I. Apachitei, Biofunctional surfaces by plasma electrolytic oxidation on titanium biomedical alloys, Surf. Eng. 32 (6) (2016) 411–417.

[2] A.A. John, S.K. Jaganathan, E. Supriyanto, A. Manikandan, Surface modification of titanium and its alloys for the enhancement of osseointegration in orthopaedics, Curr. Sci. 111 (6) (2016) 1003–1015.

[3] X. Cui, H.M. Kim, M. Kawashita, L. Wang, T. Xiong, T. Kokubo, T. Nakamura, Preparation of bioactive titania films on titanium metal via anodic oxidation, Dent. Mater. 25 (1) (2009) 80–86.

[4] R. Kumari, J.D. Majumdar, Studies on corrosion resistance and bio-activity of plasma spray deposited hydroxylapatite (HA) based TiO_2 and ZrO_2 dispersed composite coatings on titanium alloy (Ti-6Al-4V) and the same after post spray heat treatment, Appl. Surf. Sci. 420 (2017) 935–943.

[5] J.-M. Yu, H.-C. Choe, Mg-containing hydroxyapatite coatings on Ti-6Al-4V alloy for dental materials, Appl. Surf. Sci. 432 (2018) 294–299.

[6] N. Ao, D. Liu, S. Wang, Q. Zhao, X. Zhang, M. Zhang, Microstructure and tribological behavior of a TiO_2/hBN composite ceramic coating formed via micro-arc oxidation of Ti–6Al–4V alloy, J. Mater. Sci. Technol. 32 (10) (2016) 1071–1076.

[7] X. Liu, P.K. Chu, C. Ding, Surface modification of titanium, titanium alloys, and related materials for biomedical applications, Mater. Sci. Eng. R. Rep. 47 (3) (2004) 49–121.

[8] Z. Ozdemir, A. Ozdemir, G.B. Basim, Application of chemical mechanical polishing process on titanium based implants, Mater. Sci. Eng. C 68 (2016) 383–396.

[9] G. Wang, J. Li, K. Lv, W. Zhang, X. Ding, G. Yang, X. Liu, X. Jiang, Surface thermal oxidation on titanium implants to enhance osteogenic activity and in vivo osseointegration, Sci. Rep. 6 (2016) 31769.

[10] H. S, M. Ashfaq, A. T, M. Harilal, R. N, Role of electrolyte additives on in-vitro corrosion behavior of DC plasma electrolytic oxidization coatings formed on Cp-Ti, Surf. Coat. Technol. 292 (2016) 20–29.

[11] J.C.M. Souza, H.A. Tajiri, C.S. Morsch, M. Buciumeanu, M.T. Mathew, F.S. Silva, B. Henriques, Tribocorrosion behavior of Ti6Al4V coated with a bio-absorbable polymer for biomedical applications, J. Bio Tribo Corros. 1 (4) (2015) 1–6.

[12] S. Amin Yavari, Y.C. Chai, A.J. Böttger, R. Wauthle, J. Schrooten, H. Weinans, A.A. Zadpoor, Effects of anodizing parameters and heat treatment on nanotopographical features, bioactivity, and cell culture response of additively manufactured porous titanium, Mater. Sci. Eng. C 51 (2015) 132–138.

[13] S. Amin Yavari, J. van der Stok, Y.C. Chai, R. Wauthle, Z. Tahmasebi Birgani, P. Habibovic, M. Mulier, J. Schrooten, H. Weinans, A.A. Zadpoor, Bone regeneration performance of surface-treated porous titanium, Biomaterials 35 (24) (2014) 6172–6181.

[14] K. Kim, B.-A. Lee, X.-H. Piao, H.-J. Chung, Y.-J. Kim, Surface characteristics and bioactivity of an anodized titanium surface, J. Periodontal Implant Sci. 43 (4) (2013) 198–205.

[15] M. Mardali, H.R. SalimiJazi, F. Karimzadeh, B. Luthringer, C. Blawert, S. Labbaf, Comparative study on microstructure and corrosion behavior of nanostructured hydroxyapatite coatings deposited by high velocity oxygen fuel and flame spraying on AZ61 magnesium based substrates, Appl. Surf. Sci. 465 (2019) 614–624.

[16] A. Kazek-Kęsik, M. Krok-Borkowicz, G. Dercz, A. Donesz-Sikorska, E. Pamuła, W. Simka, Multilayer coatings formed on titanium alloy surfaces by plasma electrolytic oxidation-electrophoretic deposition methods, Electrochim. Acta 204 (2016) 294–306.

[17] H. Farnoush, F. Muhaffel, H. Cimenoglu, Fabrication and characterization of nano-HA-45S5 bioglass composite coatings on calcium-phosphate containing micro-arc oxidized CP-Ti substrates, Appl. Surf. Sci. 324 (2015) 765–774.

[18] S.M. Best, A.E. Porter, E.S. Thian, J. Huang, Bioceramics: past, present and for the future, J. Eur. Ceram. Soc. 28 (7) (2008) 1319–1327.

[19] L. Benea, E. Danaila, P. Ponthiaux, Effect of titania anodic formation and hydroxyapatite electrodeposition on electrochemical behaviour of Ti–6Al–4V alloy under fretting conditions for biomedical applications, Corros. Sci. 91 (2015) 262–271.

[20] C. Vasilescu, P. Drob, E. Vasilescu, I. Demetrescu, D. Ionita, M. Prodana, S.I. Drob, Characterisation and corrosion resistance of the electrodeposited hydroxyapatite and bovine serum albumin/hydroxyapatite films on Ti–6Al–4V–1Zr alloy surface, Corros. Sci. 53 (3) (2011) 992–999.

[21] P. Xiu, Z. Jia, J. Lv, C. Yin, Y. Cheng, K. Zhang, C. Song, H. Leng, Y. Zheng, H. Cai, Z. Liu, Tailored surface treatment of 3D printed porous Ti6Al4V by microarc oxidation for enhanced osseointegration via optimized bone in-growth patterns and interlocked bone/implant interface, ACS Appl. Mater. Interfaces 8 (28) (2016) 17964–17975.

[22] Y.-T. Sul, The significance of the surface properties of oxidized titanium to the bone response: special emphasis on potential biochemical bonding of oxidized titanium implant, Biomaterials 24 (22) (2003) 3893–3907.

[23] I.A.J. van Hengel, M. Riool, L.E. Fratila-Apachitei, J. Witte-Bouma, E. Farrell, A.A. Zadpoor, S.A.J. Zaat, I. Apachitei, Selective laser melting porous metallic implants with immobilized silver nanoparticles kill and prevent biofilm formation by methicillin-resistant Staphylococcus aureus, Biomaterials 140 (2017) 1–15.

[24] S. Amin Yavari, R. Wauthle, A.J. Böttger, J. Schrooten, H. Weinans, A.A. Zadpoor, Crystal structure and nanotopographical features on the surface of heat-treated and anodized porous titanium biomaterials produced using selective laser melting, Appl. Surf. Sci. 290 (2014) 287–294.

[25] E. Matykina, P. Skeldon, G.E. Thompson, Fundamental and practical evaluation of plasma electrolytic oxidation coatings of titanium, Surf. Eng. 23 (6) (2007) 412–418.

[26] K.-H. Kim, N. Ramaswamy, Electrochemical surface modification of titanium in dentistry, Dent. Mater. J. 28 (1) (2009) 20–36.

[27] F. Simchen, M. Sieber, T. Lampke, Electrolyte influence on ignition of plasma electrolytic oxidation processes on light metals, Surf. Coat. Technol. 315 (Supplement C) (2017) 205–213.

[28] M. Fazel, H.R. Salimijazi, M. Shamanian, Improvement of corrosion and tribocorrosion behavior of pure titanium by subzero anodic spark oxidation, ACS Appl. Mater. Interfaces 10 (17) (2018) 15281–15287.

[29] R.O. Hussein, X. Nie, D.O. Northwood, A. Yerokhin, A. Matthews, Spectroscopic study of electrolytic plasma and discharging behaviour during the plasma electrolytic oxidation (PEO) process, J. Phys. D. Appl. Phys. 43 (10) (2010) 105203.

[30] Y. Wang, H. Yu, C. Chen, Z. Zhao, Review of the biocompatibility of micro-arc oxidation coated titanium alloys, Mater. Des. 85 (2015) 640–652.

[31] I.d.S.V. Marques, N.C. da Cruz, R. Landers, J.C.-C. Yuan, M.F. Mesquita, C. Sukotjo, M.T. Mathew, V.A.R. Barão, Incorporation of Ca, P, and Si on bioactive coatings produced by plasma electrolytic oxidation: the role of electrolyte concentration and treatment duration, Biointerphases 10 (4) (2015) 041002.

[32] I.d.S.V. Marques, V.A.R. Barão, N.C.d. Cruz, J.C.-C. Yuan, M.F. Mesquita, A.P. Ricomini-Filho, C. Sukotjo, M.T. Mathew, Electrochemical behavior of bioactive coatings on cp-Ti surface for dental application, Corros. Sci. 100 (2015) 133–146.

[33] C.-S. Chen, Y.-L. Tsao, D.-J. Wang, S.-F. Ou, H.-Y. Cheng, Y.-C. Chiang, K.-L. Ou, Research on cell behavior related to anodized and hydrothermally treated titanium surface, Appl. Surf. Sci. 271 (2013) 1–6.

[34] V.M. Frauchiger, F. Schlottig, B. Gasser, M. Textor, Anodic plasma-chemical treatment of CP titanium surfaces for biomedical applications, Biomaterials 25 (4) (2004) 593–606.

[35] M. Montazeri, C. Dehghanian, M. Shokouhfar, A. Baradaran, Investigation of the voltage and time effects on the formation of hydroxyapatite-containing titania prepared by plasma electrolytic oxidation on Ti–6Al–4V alloy and its corrosion behavior, Appl. Surf. Sci. 257 (16) (2011) 726e8–7275.

[36] H.-J. Song, K.-H. Shin, M.-S. Kook, H.-K. Oh, Y.-J. Park, Effects of the electric conditions of AC-type microarc oxidation and hydrothermal treatment solution on the characteristics of hydroxyapatite formed on titanium, Surf. Coat. Technol. 204 (14) (2010) 2e273–2278.
[37] K. Modaresifar, S. Azizian, M. Ganjian, L.E. Fratila-Apachitei, A.A. Zadpoor, Bactericidal effects of nanopatterns: a systematic review, Acta Biomater. 83 (2019) 29–36.
[38] A.R. Ribeiro, F. Oliveira, L.C. Boldrini, P.E. Leite, P. Falagan-Lotsch, A.B.R. Linhares, W.F. Zambuzzi, B. Fragneaud, A.P.C. Campos, C.P. Gouvêa, B.S. Archanjo, C.A. Achete, E. Marcantonio Jr., L.A. Rocha, J.M. Granjeiro, Micro-arc oxidation as a tool to develop multifunctional calcium-rich surfaces for dental implant applications, Mater. Sci. Eng. C 54 (2015) 196–206.
[39] M. Shokouhfar, S.R. Allahkaram, Formation mechanism and surface characterization of ceramic composite coatings on pure titanium prepared by micro-arc oxidation in electrolytes containing nanoparticles, Surf. Coat. Technol. 291 (2016) 396–405.
[40] S. Amin Yavari, L. Loozen, F.L. Paganelli, S. Bakhshandeh, K. Lietaert, J.A. Groot, A.C. Fluit, C.H.E. Boel, J. Alblas, H.C. Vogely, H. Weinans, A.A. Zadpoor, Antibacterial behavior of additively manufactured porous titanium with nano-tubular surfaces releasing silver ions, ACS Appl. Mater. Interfaces 8 (27) (2016) 17080–17089.
[41] M. Shokouhfar, S.R. Allahkaram, Effect of incorporation of nanoparticles with different composition on wear and corrosion behavior of ceramic coatings developed on pure titanium by micro arc oxidation, Surf. Coat. Technol. 309 (2017) 767–778.
[42] M.R. Garsivaz jazi, M.A. Golozar, K. Raeissi, M. Fazel, Surface characteristics and electrochemical impedance investigation of spark-anodized Ti-6Al-4V alloy, J. Mater. Eng. Perform. 23 (4) (2014) 1270–1278.
[43] A.L. Yerokhin, X. Nie, A. Leyland, A. Matthews, S.J. Dowey, Plasma electrolysis for surface engineering, Surf. Coat. Technol. 122 (2) (1999) 73–93.
[44] X. Zhang, K.S. Vecchio, Hydrothermal synthesis of hydroxyapatite rods, J. Cryst. Growth 308 (1) (2007) 133–140.
[45] B.S. Necula, L.E. Fratila-Apachitei, S.A.J. Zaat, I. Apachitei, J. Duszczyk, In vitro antibacterial activity of porous TiO_2–Ag composite layers against methicillin-resistant Staphylococcus aureus, Acta Biomater. 5 (9) (2009) 3573–3580.
[46] D.D. Deligianni, N.D. Katsala, P.G. Koutsoukos, Y.F. Missirlis, Effect of surface roughness of hydroxyapatite on human bone marrow cell adhesion, proliferation, differentiation and detachment strength, Biomaterials 22 (1) (2000) 87–96.
[47] Y.S. Cho, J.S. Lee, M.W. Hong, S.-H. Lee, Y.Y. Kim, Y.-S. Cho, Comparative assessment of the ability of dual-pore structure and hydroxyapatite to enhance the proliferation of osteoblast-like cells in well-interconnected scaffolds, Int. J. Precis. Eng. Manuf. 19 (4) (2018) 605–612.
[48] M. Nakamura, A. Nagai, T. Hentunen, J. Salonen, Y. Sekijima, T. Okura, K. Hashimoto, Y. Toda, H. Monma, K. Yamashita, Surface electric fields increase osteoblast adhesion through improved wettability on hydroxyapatite electret, ACS Appl. Mater. Interfaces 1 (10) (2009) 2181–2189.
[49] M. Babaei, C. Dehghanian, M. Vanaki, Effect of additive on electrochemical corrosion properties of plasma electrolytic oxidation coatings formed on CP Ti under different processing frequency, Appl. Surf. Sci. 357 (Part A) (2015) 712–720.